Combined Molecular Dynamics and Φ-Value Analysis of Structure−Reactivity Relationships in the Transition State and Unfolding Pathway of Barnase: Structural Basis of Hammond and Ant...

ARTICLE *in* JOURNAL OF THE AMERICAN CHEMICAL SOCIETY · DECEMBER 1998

Impact Factor: 12.11 · DOI: 10.1021/ja981558y

3 AUTHORS, INCLUDING:

Valerie Daggett
University of Washington Seattle
222 PUBLICATIONS **12,462** CITATIONS
SEE PROFILE

Alan Fersht
University of Cambridge
628 PUBLICATIONS **52,291** CITATIONS
SEE PROFILE

Combined Molecular Dynamics and Φ-Value Analysis of Structure−Reactivity Relationships in the Transition State and Unfolding Pathway of Barnase: Structural Basis of Hammond and Anti-Hammond Effects

Valerie Daggett,*,† Aijun Li,† and Alan R. Fersht*,‡

Contribution from the Department of Medicinal Chemistry, University of Washington, Seattle, Washington 98195-7610, and University Chemical Laboratories, Lensfield Road, University of Cambridge, Cambridge CB2 1EW, United Kingdom

Received May 5, 1998. Revised Manuscript Received October 7, 1998

Abstract: The folding/unfolding pathway of barnase has been analyzed using a method similar to the classical Brønsted-β approach: Φ-value analysis. Kinetic and equilibrium measurements on the folding/unfolding of over 100 designed mutants have led to a residue-by-residue description of the transition state. The transition state responds to mutation and changes in solvent in a manner analogous to both classical Hammond and anti-Hammond behavior as the energy landscape is perturbed. Here, we compare the Φ-value analysis with an explicit structural analysis of the transition state by molecular dynamics simulations of thermal denaturation of wild-type and two mutant forms of barnase. We look for similarities in the results of experiment and simulation to provide a detailed and reliable description of the folding reaction and for differences that could point to deficiencies in the methods. In general, there is excellent agreement between simulation and experiment, with a correlation coefficient of 0.93 between observed and simulated Φ-values for the transition state for unfolding, with the exception of the second helix, α2. In the simulations, wild-type barnase unfolded by disruption of the hydrophobic cores and β-structure, followed by unraveling of the principal α-helix, α1. The Ile 88 → Val mutant unfolded by the same mechanism as the wild-type protein, albeit more rapidly. Tyr 17 is one of the residues that, when mutated, leads to anti-Hammond effects; the helix unfolds earlier, relative to gross unfolding of the rest of the protein. In the simulation of the unfolding of the Tyr 17 → Gly mutant, the main helix unraveled before substantial loss of β-structure, showing more precisely the structural change in the transition state. The major difference between simulation and experiment is that α2 is present in the simulated transition state, but Φ-values suggest that it is unstructured. Although this could result from simulation overestimating the helical content, there is an alternative explanation that reconciles simulation and experiment. The segment of protein containing α2 is autonomous and makes few interactions with the body of the protein in the simulated transition state. If the folding of a segment of the protein is not coupled to the rest of the molecule, then the mutations may not be felt until significant interactions are made between these portions of the protein. Such an effect could occur for any multimodular protein.

Introduction

A number of technical advances is making it possible to characterize the protein folding process and intermediates that are populated en route. Experiment provides the lead with low- to high-resolution glimpses into the process, while molecular dynamics simulations can provide structural and dynamic information at atomic resolution. The two approaches are highly complementary, such that theory can be used to fill in the experimental gaps and provide structural information unobtainable by experiment, provided it has been demonstrated that the simulations are reasonable and in agreement with experiment. Such synergism is important in the study of transition states, whose characterization is particularly challenging but required for a comprehensive description of the folding pathway.[1] In addition, for proteins that fold by a two-state mechanism, characterization of transition states is crucial since other partially folded intermediates are unobservable.

The only way to obtain experimental information about transition states is from kinetics. The transition state is an ensemble of structures, as the barrier involves the breakage and formation of many weak noncovalent interactions. Fersht and co-workers[2] have developed an approach, termed the protein engineering method, in which mutations are made throughout a protein and the resulting energetic consequences are measured. This approach is analogous to structure−activity studies in physical organic chemistry via linear free energy relationships. The mutations, or substituents, act as probes, such that the structure at the site of mutation can be inferred from the energetics. More specifically, determination of the structure of the transition state is based on a quantity Φ, which is analo-

† University of Washington.
‡ University of Cambridge.

(1) Fersht, A. R. *Curr. Opin. Struct. Biol.* **1995**, *5*, 79−84.
(2) Fersht, A. R.; Matouschek, A.; Serrano, L. *J. Mol. Biol.* **1992**, *224*, 771−782.

10.1021/ja981558y CCC: $15.00
Published on Web 12/02/1998

gous but not identical to the Brønsted β value. Φ is calculated from the following equation,[2,3]

$$\Phi_F = \frac{\Delta G_{\ddagger-D} - \Delta G'_{\ddagger-D}}{\Delta G_{N-D} - \Delta G'_{N-D}} = \frac{\Delta\Delta G_{\ddagger-D}}{\Delta\Delta G_{N-D}} \quad (1)$$

where $\Delta G_{\ddagger-D}$ and ΔG_{N-D} are the free energies of the transition and native states, respectively, relative to the unfolded, denatured state of the wild-type protein. The corresponding terms for the mutant are indicated by a prime. $\Delta\Delta G_{N-D}$ and $\Delta\Delta G_{\ddagger-D}$ are the destabilization energies of the native and the transition states, respectively, caused by mutation. In the direction of folding, Φ is termed Φ_F and that for unfolding, Φ_U ($\Phi_F = 1 - \Phi_U$). Consider a case where, in the transition state of unfolding, the structure of the protein at the site of mutation is the same as that in the native state. Then, the transition state is destabilized by exactly the same amount as the native state; that is, $\Delta\Delta G_{\ddagger-D} = \Delta\Delta G_{N-D}$ and $\Phi_F = 1$. In contrast, a Φ_F value of 0 implies that the structure of the transition state at the site of mutation is the same as that in the unfolded state. Intermediate values could result from a mixture of pathways or represent structures that are partially unfolded in the transition state. Thus, structure is inferred from energetics using this approach, and it has now been applied to several systems: barnase,[3−7] chymotrypsin inhibitor 2 (CI2),[7−10] the P22 Arc repressor,[11] iso-1-cytochrome *c*,[12] CheY,[13] and barstar.[14] Fersht et al.[10] have devised a test to show that partial Φ-values for CI2 and barnase represent partial structure formation and not parallel pathways.

The transition state for a folding/unfolding process is inherently complicated. The transition state is not localized to a particular bond as in a chemical reaction because of the large number of noncovalent interactions affected. So, one cannot just consider enthalpic, or potential energy, barriers; entropy must also be included. This means that the major transition state is the ensemble of structures with the highest free energy on the pathway. Unfortunately, even if a reasonable unfolding pathway can be simulated with molecular dynamics, the calculation of free energies for such a complicated process is not possible. So, instead we rely on structural properties to identify the transition state in a simulation.[15,16] Using this approach, structural attributes of the transition-state ensemble can be precisely delineated; but, there is no guarantee that the state identified is the state of highest free energy. Therefore, there is potential for synergy between experimental and theoretical efforts to characterize partially folded, transient forms of proteins, such as transition states, where conventional structure determination methods are limited. In our previous simulations, good agreement was obtained with experiment for the unfolding of CI2.[15−18] CI2 is the archetypal small protein of 64 residues that folds as a single cooperative unit according to two-state kinetics.[19] We now focus on a more complex protein, barnase (Figure 1). Barnase contains 110 residues and folds according to multistate kinetics.

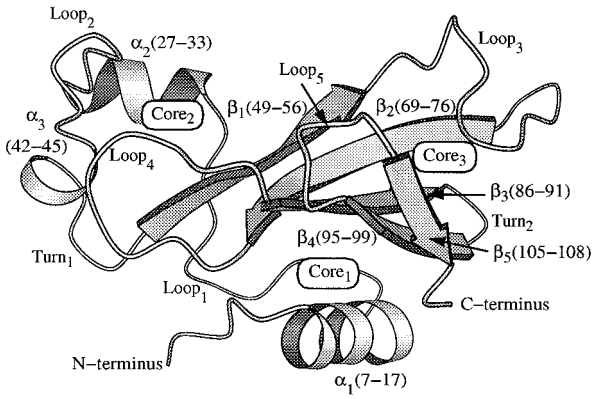

Figure 1. Main-chain fold of the barnase NMR structure[25] with the positions of secondary structure elements indicated. The secondary structure was identified using a method based on main-chain dihedral angles.[52,53]

Although an atomic-level model of the transition state of unfolding of barnase generated from a molecular dynamics simulation should further define the unfolding pathway of this protein, the sensitivity of the transition state and unfolding pathway to mutation is also of interest. Recently, Fersht and co-workers[5−7] have shown that mutations and changes in the environment can slide the transition state both along and perpendicular to the reaction pathway. Again, the use of linear free energy relationships, analogous to the Brønsted equation to evaluate structure−reactivity effects in physical organic chemistry, has been critical to this analysis. Specifically, the equilibrium and activation free energies of unfolding are generally linearly related to the concentration of denaturant:

$$\Delta G_{D-N} = \Delta G^{H_2O}_{D-N} - m_{D-N}[\text{denaturant}] \quad (2)$$

$$\Delta G_{\ddagger-N} = \Delta G^{H_2O}_{\ddagger-N} - m_{\ddagger-N}[\text{denaturant}] \quad (3)$$

where the subscript notation is described above. ΔG_{D-N} and $\Delta G_{\ddagger-N}$ with the H_2O superscript are values extrapolated to pure water, and m values are constants for a particular protein and are generally considered to reflect the change in solvent exposure between the designated states. Combination of eqs 2 and 3 gives

$$\partial(\Delta G_{\ddagger-N})/\partial(\Delta G_{D-N}) = m_{\ddagger-N}/m_{D-N} = \beta_T \quad (4)$$

The ratio of $m_{\ddagger-N}/m_{D-N}$ corresponds to a Brønsted β value, which we call β_T. β_T is an index of the position of the transition state along the reaction pathway, as defined by the change in solvent exposure upon unfolding to the transition state.[20] We use β_T in the direction of unfolding since it can be measured

(3) Matouschek, A.; Kellis, J. T., Jr.; Serrano, L.; Fersht, A. R. *Nature* **1989**, *340*, 122−126.
(4) Serrano, L.; Matouschek, A.; Fersht, A. R. *J. Mol. Biol.* **1992**, *224*, 805−818.
(5) Matouschek, A.; Fersht, A. R. *Proc. Natl. Acad. Sci. U.S.A.* **1993**, *90*, 7814−7818.
(6) Matthews, J. M.; Fersht, A. R. *Biochemistry* **1995**, *34*, 6805−6814.
(7) Matouschek, A.; Otzen, D. E.; Itzhaki, L. S.; Jackson, S. E.; Fersht, A. R. *Biochemistry* **1995**, *34*, 13656−13662.
(8) Itzhaki, L. S.; Otzen, D. E.; Fersht, A. R. *J. Mol. Biol.* **1995**, *254*, 260−288.
(9) Otzen, D. E.; Itzhaki, L. S.; elMasry, N. F.; Jackson, S. E.; Fersht, A. R. *Proc. Natl. Acad. Sci. U.S.A.*. **1994**, *91*, 10422−10425.
(10) Fersht, A. R.; Itzhaki, L. S.; elMasry, N. F.; Matthews, J. M.; Otzen, D. E. *Proc. Natl. Acad. Sci. U.S.A.* **1994**, *91*, 10426−10429.
(11) Milla, M. E.; Brown, B. M.; Waldburger, C. D.; Sauer, R. T. *Biochemistry* **1995**, *34*, 13914−13919.
(12) Doyle, D. F.; Waldner, J. C.; Parikh, S.; Alcazar-Roman, L.; Pielak, G. J. *Biochemistry* **1996**, *35*, 7403−7411.
(13) Lopez-Hernandez, E.; Serrano, L. Folding Des. **1996**, *1*, 43−55.
(14) Nolting, B.; Golbik, R.; Neira, J. L.; Soler-Gonzalez, A.; Schreiber, G.; Fersht, A. R. *Proc. Natl. Acad. Sci. U.S.A.* **1997**, *94*, 826−830.
(15) Li, A.; Daggett, V. *Proc. Natl. Acad. Sci. U.S.A.* **1994**, *91*, 10430−10434.
(16) Li, A.; Daggett, V. *J. Mol. Biol.* **1996**, *257*, 412−429.
(17) Daggett, V.; Li, A.; Itzhaki, L. S.; Otzen, D. E.; Fersht, A. R. *J. Mol. Biol.* **1996**, *257*, 430−440.
(18) Ladurner, A. G.; Itzhaki, L. S.; Daggett, V.; Fersht, A. R. *Proc. Natl. Acad. Sci. U.S.A.* **1998**, *95*, 8473−8478.
(19) Jackson, S. E.; Fersht, A. R. *Biochemistry* **1991**, *30*, 10428−10435.
(20) Tanford, C. *Adv. Protein Chem.* **1970**, *24*, 1−95.

for proteins with intermediates on the pathway. Also, it is worth noting that, for barnase, the major rate-limiting transition state of folding is identical to the transition state of unfolding.[3,4]

Most mutations in the major core of barnase and the first α-helix, α1 (Figure 1), show Hammond-type behavior.[5] That is, destabilization due to mutation decreases the energy difference between the transition and native states and moves the transition state closer to the native state.[21] More recent studies of the sensitivity of the transition state to mutations in both α1 and α2 by Matthews and Fersht[6] describe an interesting mutant, Tyr 17 → Gly. In this case, the β_T value drops from 0.33 to 0.29, indicative of Hammond behavior. However, the Φ values within the helix decrease, suggesting that although the overall nature of the transition state is more nativelike for Y17G, α1 becomes less structured. This paradoxical effect is referred to as anti-Hammond behavior (see Matthews and Fersht[6] for further discussion regarding the Hammond postulate formalism). These intriguing results led us to simulate the unfolding of the wild-type, Y17G, and I88V (chosen as a control because it is in core 1 and shows little Hammond behavior) proteins in the hope of elucidating the effects of the mutations on the transition state and unfolding pathway.

Methods

Molecular dynamics simulations were performed using the program ENCAD.[22] The potential energy function and MD protocols have been described elsewhere.[23,24] Each molecular system simulated was described using an all-atom representation of both the protein and the solvent. The average NMR solution structure[25] was used as the starting structure for the simulations. Residual strain in the structure was relieved using 1000 steps of conjugate gradient minimization. The I88V and Y17G mutants were constructed from the resulting structure by swapping in the appropriate side chain with maintenance of the original side-chain orientation insofar as possible. Then, another 10 steps of minimization were performed. Side-chain protonation states were chosen to mimic low-neutral pH (Lys, Arg, and His were positively charged, and Asp and Glu were negatively charged). The protein was then solvated using a box extending at least 8 Å in all directions. Periodic boundary conditions were employed to reduce edge effects and simulate a semidilute solvent environment. The solvent was then subjected to 1000 cycles of minimization, 2 ps of MD, and another 1000 steps of minimization. This water preparation was followed by 1000 steps of minimization of the protein and then 1000 steps of minimization of the full protein−solvent system. The water density was set to the experimental value at 498 K of 0.829 g/cm^3 to relieve excess pressure.[24,26] This density corresponds to the lowest pressure (∼26 atm) required for water to stay in the liquid phase at 498 K.[27] The lower density was obtained by expansion of the box to extend ∼10 Å from any protein atom. After the preparatory steps described above, the systems were heated to 498 K. Initial atomic velocities were chosen using a Maxwellian distribution. Velocities were periodically scaled until the target temperature was reached, typically 2−3 ps. At this point, classical MD simulations were performed in the NVE microcanonical ensemble. Each simulation was carried out for 2 ns using a 2-fs integration time step (2000 ps, or 10^6 iterations). An 8-Å nonbonded cutoff was used, and the nonbonded list was updated every five cycles. 10 000 structures were saved for analysis (five per picosecond). To check that the results were reproducible, an independent simulation of the wild-type protein (denoted WT TS2, compared with WT TS1 for the main simulation beginning from the NMR structure) was performed beginning from the crystal structure[28] using the protocols described above. In addition, a control simulation was performed of the wild-type protein at 298 K and has been presented by Li and Daggett,[29] along with a more complete description of the unfolding pathway of the wild-type protein at 498 K.

Results

Description of the Unfolding of Wild-Type Barnase and the Y17G and I88V Mutants. Thermal unfolding of the wild-type and two mutant forms of barnase, Y17G and I88V, is depicted in Figure 2A by the movement of the structures away from their respective starting structures. All three proteins deviated significantly during the first 200 ps of each simulation, but their behavior differed, with the mutants unfolding more rapidly. For wild type and Y17G, this difference diminished from 200 to 900 ps; however, the RMS deviation of I88V remained higher throughout this time period. Late in the simulation, the differences were mostly due to shape changes, with the mutants being more compact: at 2 ns (2000 ps), the radius of gyration for wild type, Y17G, and I88V was 16.6, 15.5, and 15.3 Å, respectively.

The loss of secondary and tertiary structure also differed for the wild-type and mutant proteins early in the unfolding simulation. From 50 to 200 ps, the wild-type and Y17G proteins had comparable degrees of tertiary packing, but the secondary structure content of Y17G was approximately 13% lower (Figure 2B). In contrast, the I88V mutation resulted in a decrease in both tertiary and secondary structure over the first 500 ps (Figure 2B). Late in the simulations, all three proteins made approximately the same number of tertiary contacts, while Y17G stood out with a lower secondary structure content than the wild-type and I88V proteins.

A breakdown of the loss of secondary structure into α-helical and β-sheet components is given in Figure 3. Both the wild-type and I88V proteins showed a roughly similar loss of helical and β-structure, except for the loss and recovery of helical structure experienced early on by the wild-type protein. After a 20−40% loss of helical content, the movement was mostly in the direction of β-sheet loss for both wild type and I88V, seen as the off-diagonal motion upward. After disruption of the β-structure, there was further, but incomplete, loss of helical structure. The main difference between these two proteins was the rate of structure loss, with I88V unfolding more rapidly. In contrast, the helical structure was less stable in the Y17G mutant, with early movement primarily in the direction of helix loss. After the helix content dropped to ∼50%, the β-content dropped by ∼25%, and then the helix fell apart and β-structure was lost. Though there was momentary recovery of the helix, the overall trend was that loss of the helix preceded loss of the β-sheet. That the motion in each case does not fall along the diagonal indicates that the secondary structure units act semi-independently as unfolding proceeds, especially after the loss of ∼50% of the β- and α-structures. By removing the time component (or embedding it), this projection of secondary structure illustrates that the wild-type and I88V proteins unfold in a similar manner, albeit at a different rate. Y17G appears to follow a similar path initially but then unfolds by a different mechanism. Snapshots taken from the simulations illustrate some of these structural differences (Figure 4).

(21) Hammond, G. S. *J. Am. Chem. Soc.* **1955**, *77*, 334−338.
(22) Levitt, M. *ENCAD, Computer Program*; Energy Calculations and Dynamics; Molecular Applications Group, Palo Alto, CA, and Yeda, Rehovot, Israel, 1990.
(23) Levitt, M.; Hirshberg, M.; Sharon, R.; Daggett, V. *Comput. Phys. Commun.* **1995**, *91*, 215−231.
(24) Levitt, M.; Hirshberg, M.; Sharon, R.; Laidig, K. E.; Daggett V. *J. Phys. Chem.* **1997**, *101*, 5051−5061.
(25) Bycroft, M.; Ludvigsen, S.; Fersht, A. R.; Poulsen, F. M. *Biochemistry* **1991**, *30*, 8697−8701.
(26) Kell, G. S. *J. Chem. Eng. Data* **1967**, *12*, 66−68.
(27) Haar, L.; Gallagher, J. S.; Kell, G. S. *NBS/NRC Steam Tables*; Hemisphere Publication Corp.: Washington, DC, 1984.
(28) Baudet, S.; Janin, J. *J. Mol. Biol.* **1991**, *219*, 123−132.
(29) Li, A.; Daggett, V. *J. Mol. Biol.* **1998**, *275*, 677−694.

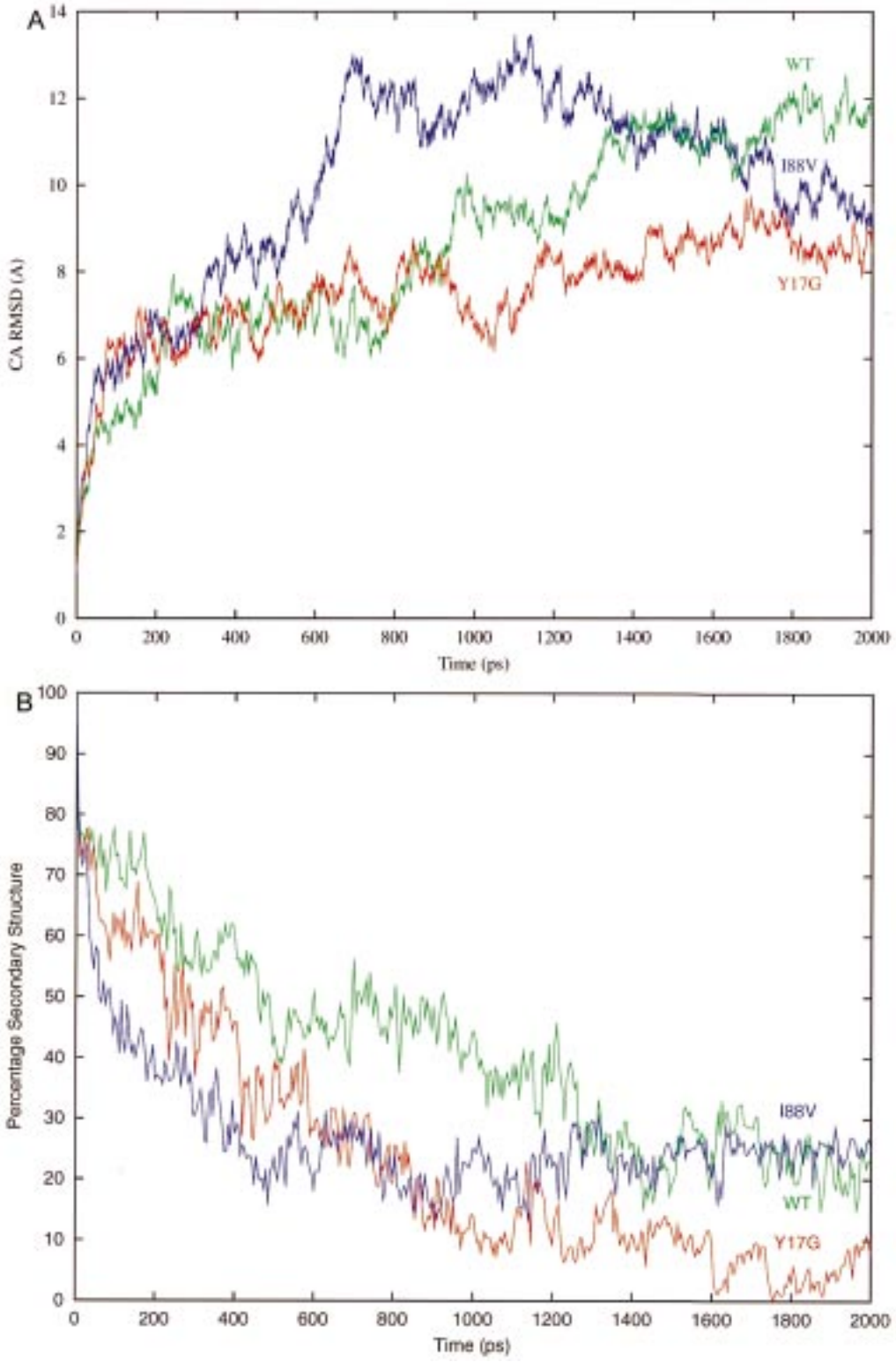

Figure 2. (A) C_α root-mean-square deviation from the starting NMR structure[25] as a function of simulation time for the wild-type, Y17G, and I88V proteins. The deviation was calculated after optimal superposition of structures.[51] (B) Percentage of native secondary structure as a function of simulation time, using the method described in the legend to Figure 1.

The helical content of the main α-helix, α1, is shown in Figure 5. α1 was destabilized upon mutation of Tyr 17→ Gly, while the helix content in the wild-type and I88V proteins remained high throughout most of the simulations (Figures 4 and 5). The β-structure of wild-type barnase was already completely disrupted by the time the helix unfolded (Figure 3). In contrast, the helix content of the Y17G mutant was lower at the beginning of the simulation, and α1 completely unfolded by 850 ps (Figures 3−5).

From the gross measures of structure presented above, the mutations were not innocuous. Instead, the I88V mutation destabilized the structure such that the protein unfolded more rapidly, but by a pathway similar to that of wild type. For Y17G, the mutation destabilized a particular element of structure such

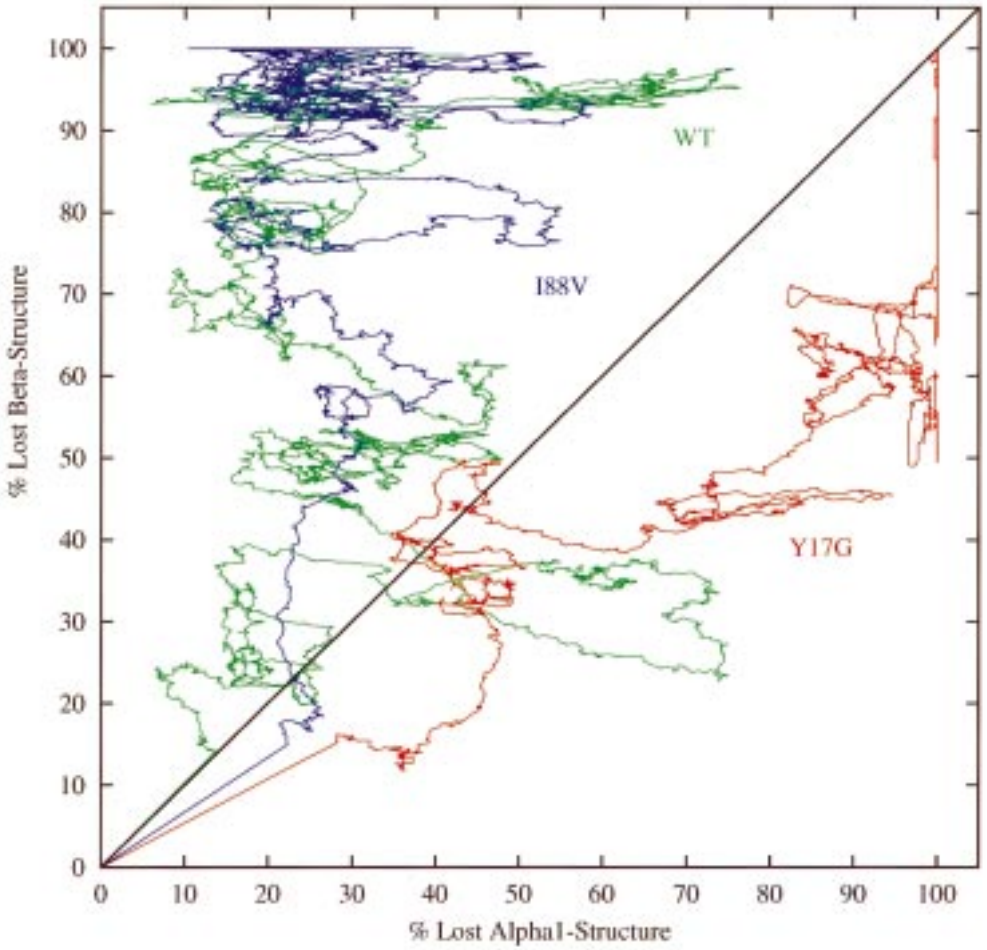

Figure 3. Loss of β-structure and helical content of α1. The points are connected sequentially in time and show the order of secondary structure loss. Secondary structure content was assessed as described in the legend to Figure 1.

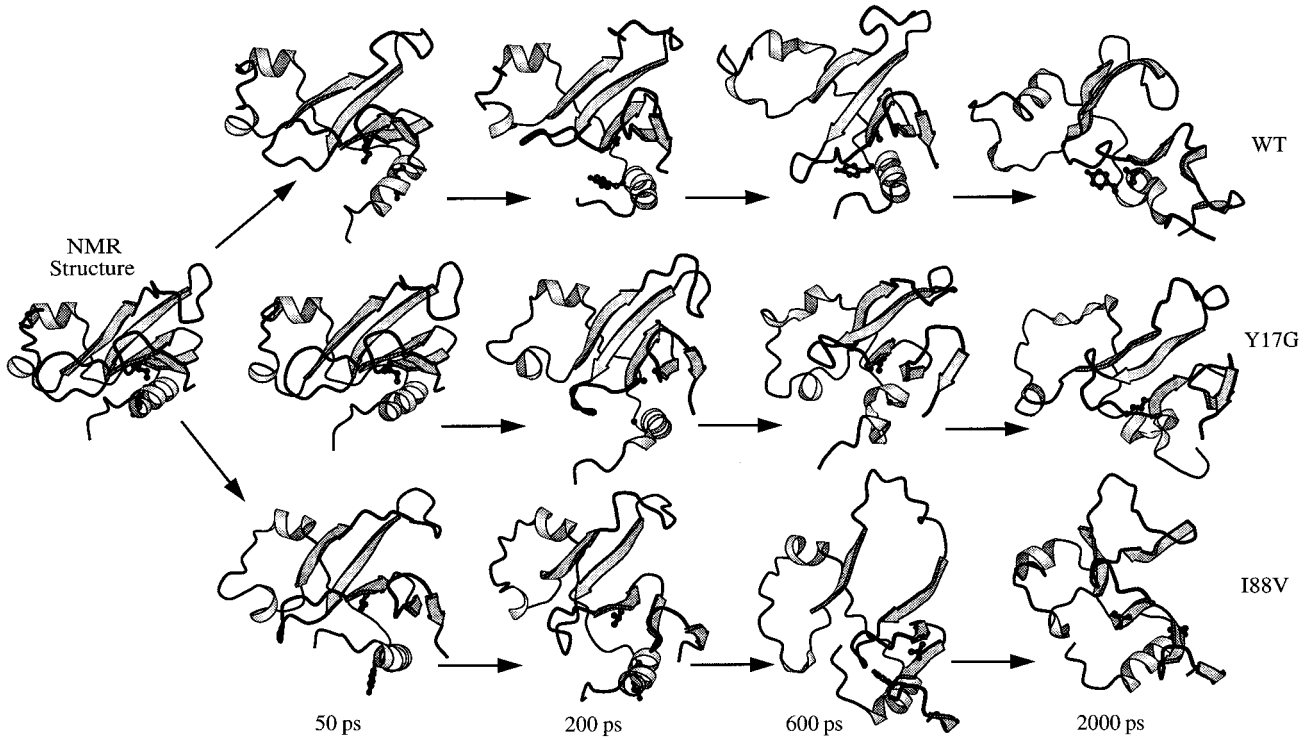

Figure 4. Structures extracted from the simulations over time. Residues 17 and 88 are shown explicitly in black.

that the protein unfolded by a different mechanism with respect to the loss of secondary structure. It is then of interest to see whether this is the case if one probes more deeply and delineates how the mutations affect the structure. In the case of the I88V

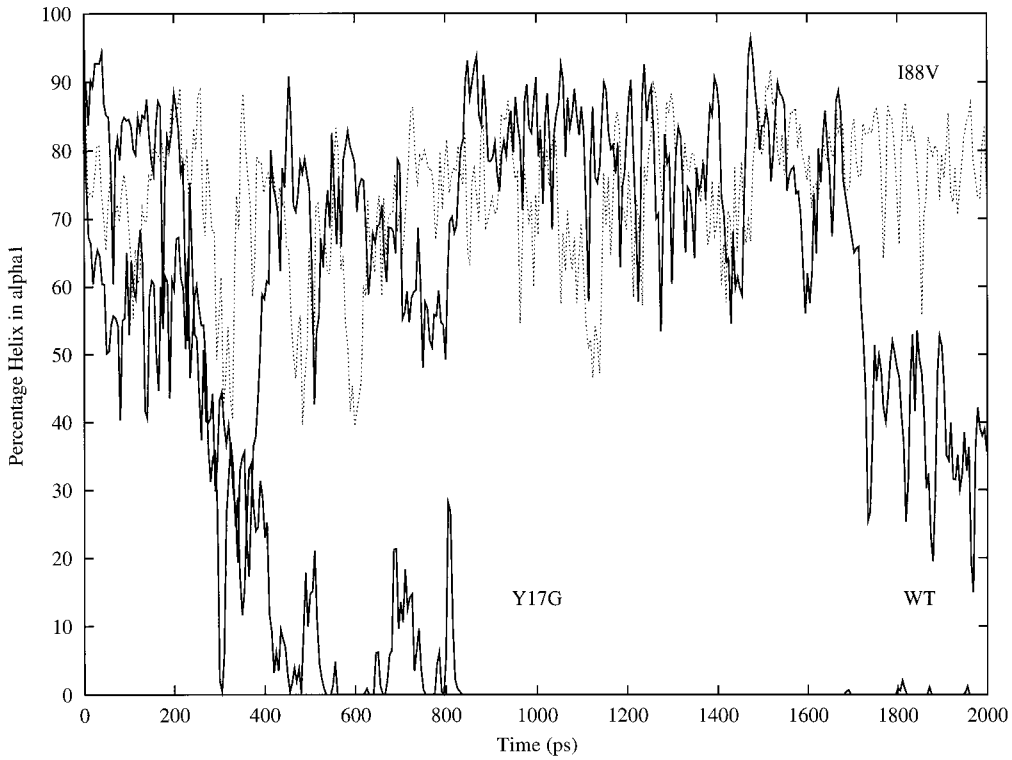

Figure 5. Percentage of helical structure of α1 as a function of simulation time. Helical content was assessed as described in the legend to Figure 1.

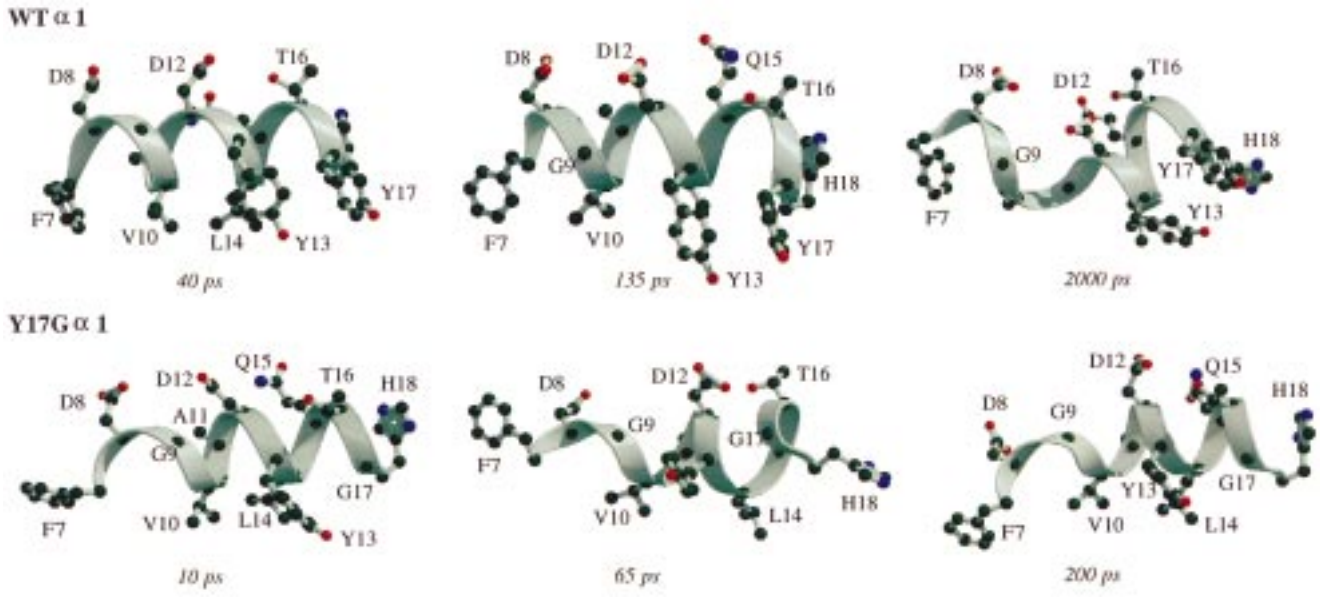

Figure 6. Snapshots from the Y17G simulation illustrating the unfolding of α1.

mutant, the mechanism of unfolding was similar to that of wild type. However, the mutation disrupted packing interactions in the main hydrophobic core between the β-sheet and α1 (Figure 4). The disruption led to earlier and more extensive damage of the β-sheet. The effects of the Y17G mutation were more complex.

The first major step in the unfolding of Y17G was the unwinding of residues 7−10. There were a variety of factors involved in destabilization of this portion of the helix, including electrostatic repulsion between Asp 8 and Asp 12, steric crowding of Val 10 with Tyr 13 and Leu 14, and the presence of a Gly at position 9. In contrast, a variety of side-chain interactions stabilize the rest of the helix, including those between Ala 11 and Leu 14, Asp 12 with Gln 15 and Thr 16, and Tyr 13 with Tyr 17. Extension of the N-terminus of the helix due to the two main repulsive interactions was facilitated by rotation about Gly 9. In turn, after the separation of the Asp residues, Asp 12 formed a hydrogen bond with Thr 16, breaking the Thr 16 hydrogen bond with the main-chain carbonyl of Asp 12, which re-formed periodically during the simulations (Figure 6). These interactions required some distortions to the main chain of residue 16, which were facilitated in the Gly 17 mutant. After the unwinding of the N-terminus, some further distortions to the main chain of residues 16 and 17 occurred in all simulations due to movements of residues 17, 18, and 19 to cap the helix, which occurred readily in the more flexible Gly

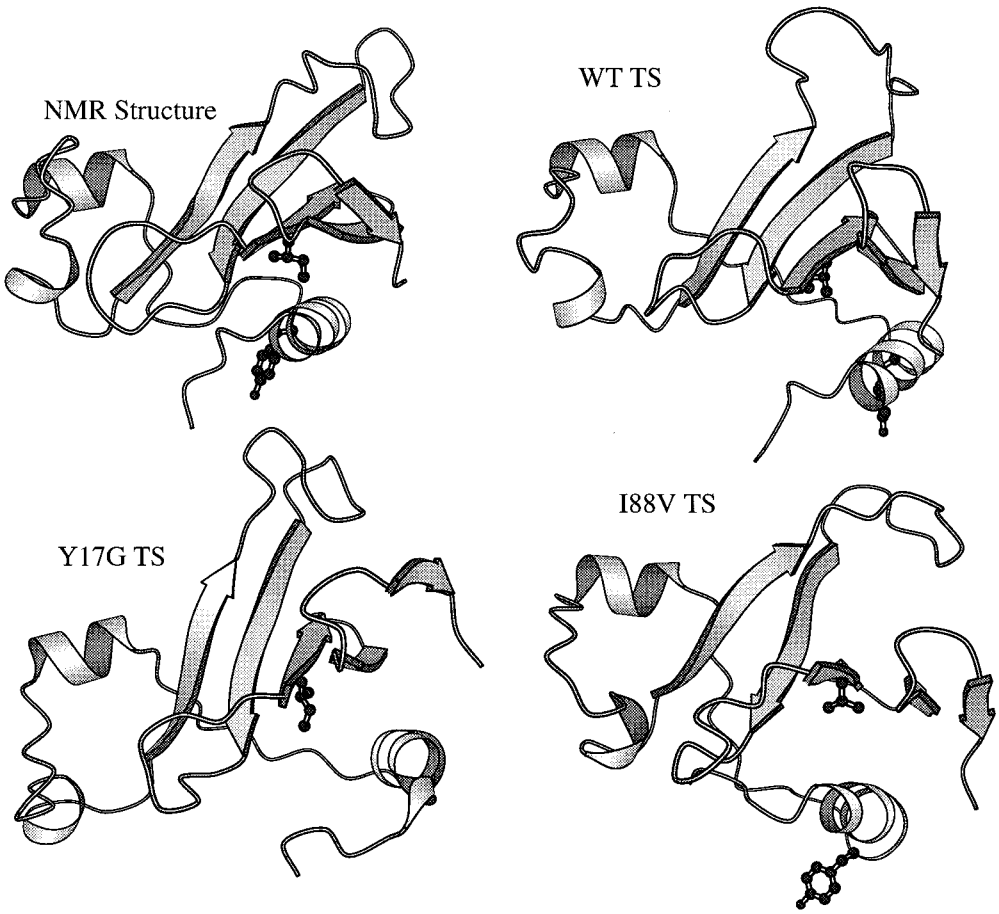

Figure 7. Main-chain fold of the transition-state models generated in the simulations. The average structures from the following time periods are depicted: 135−140 ps, WT; 65−70 ps, Y17G; and 63−68 ps, I88V.

17 mutant. These capping interactions involved nonnative and nonhelical main chain hydrogen bonds (i.e., $i \rightarrow i + 3$ and $i \rightarrow i + 5$), which both stabilized the compact structure and distorted the helix. The consequences of the Tyr 17 → Gly mutation, as well as the loss of the packing interactions between Tyr 13 and Tyr 17 (Figure 6), led to complete loss of the helix after approximately 800 ps.

Characterization of the Transition State of Unfolding. The major transition state in unfolding corresponds to the highest free energy barrier. Unfortunately, reliable free energy changes cannot be computed from a simulation for a process as complicated as protein unfolding in solution. Therefore, we are forced to rely on other approaches to identify potential transition-state structures from simulations. We make use of a conformational clustering method.[15−16,29] Using this approach, all structures from a simulation are compared with all other structures, and a full matrix of RMS deviations is constructed. This matrix describes the conformations in $n \times n$-dimensional space, where $n = 10\,000$ for these simulations (2000 ps × 5 structures/ps). We then project from high-dimensional space to two or three dimensions. The resulting projections are an approximate fit to the high-dimensional results. Similar structures will appear as clusters in the reduced projections. The projections consist of a series of points connected in time, such that points close in space correspond to similar conformations. The distance between points gives the approximate RMSD between the corresponding structures. Using this approach, conformational clusters or substates can be easily identified.

To model the transition state, we use those structures from the simulation immediately prior to the first major conformational change during unfolding as identified in the RMSD projections (see Li and Daggett[15,16] for further discussion). We have defined the transition-state region in this way by reasoning that one can obtain a high free energy of activation for a process when the enthalpy increases and the entropy changes very little. We reason that a protein may not succeed in every attempt to pass over the barrier, but once it does the structure should change quickly, the entropy will increase, and the free energy will drop. This method is not rigorous, but it can provide *testable* transition-state structural models. This approach yields the structures in the following time periods as transition-state models: the 135−140-ps time period of the wild-type simulation (shown as the first small cluster in Figure 4 of Li and Daggett[29]), 65−70 ps of the Y17G simulation, and 63−68 ps from the I88V simulation (Figure 7).

The wild-type transition-state model has a 4.7-Å RMSD from the NMR starting structure, while the mutants deviated more but occurred earlier in the simulation (Table 1). The RMS deviations between the different transition-state models were of the same magnitude, ∼4.5 Å. This is similar to the spread observed between wild-type transition-state models of CI2 generated in four independent simulations.[16] For comparison, the RMSD between the 2000-ps structures shown in Figure 4 was 10.3−11.5 Å. The average structures of the transition states were similar, as shown in Figure 7. They differed primarily as would be expected from their effects on the unfolding process, as discussed above. That is, α1 is disrupted in the Y17G transition state (Figure 7, Table 1, and see the 65-ps snapshot in Figure 6), and the β-sheet is slightly more disrupted in the I88V transition state (Figure 7 and Table 1). Interestingly, the

Table 1. Properties of the Unfolding Transition States for Wild-Type and Mutant Barnase

property	WT TS1	WT TS2	Y17G TS	I88V TS
time (ps)	135−140	185−190	65−70	63−68
Cα RMSD to N (Å)[a]	4.8	5.2	5.3	5.2
Cα RMSD to WT TS1 (Å)[a]		5.4	4.6	4.7
<α-helix content> (res.)[b]	16	13	15	15
<α1 helix content> (res.)[b]	10	8	5	10
<β-sheet content> (res.)[b]	23	20	29	21
<ΔSASA, calc>[c] (%)	33	32	29	32
<ΔSASA, expt>[d] (%)	33	33	29	31
<% native tertiary contacts>[e]	74	66	74	69

[a] The Cα RMS deviation from the NMR structure (N) and average wild-type transition-state structure (WT TS1) was calculated after removal of rotational and translational motion using the method of Kabsch.[51] WT TS1 refers to the main transition state discussed in the text from the simulation beginning from the NMR structure. WT TS2 refers to the second simulation beginning from the crystal structure. The average transition-state structures were minimized briefly (500 steps) in vacuo to remove any bad contacts. [b] The secondary structure determinations are based on repeating (ϕ,φ) values (at least three consecutive residues must have the appropriate dihedral angles).[52,53] The structure content is given in units of residues and represents the average native secondary structure over the time period indicated. The α1 content is the number of α1 residues in the helical region of (ϕ,φ) space in the average transition-state structures. [c] The change in solvent-accessible surface area (SASA) is defined as the relative difference between the average accessible surface area for the transition-state ensemble relative to the NMR structure (6356 Å^2). The surface areas were calculated using NACCESS.[54] [d] Experimental values are given for m_+/m extrapolated to pure water (Matthews and Fersht[6] and Dalby et al.[33]) [e] The percentage of native heavy atom contacts in the TS is relative to the NMR structure, with 335 contacts. A contact is defined as having carbon−carbon distances of ≤5.4 Å, and all other pairs must be ≤4.6 Å.

β-content of the Y17G transition state was substantially higher than those of wild type and I88V. Nevertheless, neither of these mutations caused drastic changes in the overall topology of the transition state (Figure 7). The change in solvent-accessible surface area of the wild-type and I88V transition states to the native state were similar, but Y17G had less exposed surface area (Table 1), as has been observed experimentally (Table 1). Despite the general increase in solvent accessibility and expansion of the protein in the transition state, the core was not filled with water.

All three transition-state models have diminished tertiary contacts relative to those of the native state (Table 1 and Figure 8). The differences and similarities were not uniform throughout the protein. For example, in the Y17G model, packing interactions in core 1 were disrupted relative to the wild-type transition state, while those in cores 2 and 3 were comparable and even slightly stronger (compare Figure 8B and C). Diminished packing in core 1 is not surprising, given the disruption in α1 (Figure 6), which resulted in the extension of the N-terminal portion of the helix away from the core (Figures 6−8). In contrast, core 2 is disrupted in the I88V transition-state model, yet interactions within core 1 improved (Figure 8D). Interestingly, many of the packing interactions within core 3 of I88V were between side-chain and main-chain atoms, in contrast to the wild-type and Y17G proteins. The side-chain−side-chain packing interactions decreased by 15% upon introduction of Val 88 (for I88V, there was a 70% drop in interactions relative to the native state versus a 55% drop for the wild-type transition-state model).

The extent and position of the loop structure was comparable in the three transition states (Figure 7). Loop 1 was in all cases extended by at least 6 Å (the distance between the Cα atoms of residues 18 and 26 was monitored) compared to that in the NMR structure. Loop 2 retained a more compact conformation but pulled away from the protein. Loop 3 forms a flap over the active site of barnase (Figure 1). The flap opened in the wild-type transition state but remained more closely packed against the protein in the mutant transition states (Figure 7). Despite the movement of loop 3, the position of His 102 relative to the floor of the active site formed by the β-sheet was roughly retained (Figure 9). Loop 3 moved down toward the center of the protein, shifting Glu 60, but Glu 60 and His 102 remain near in space, spanning the active-site cleft (Figure 9). The docking between the N-terminal end of α2 and the β-sheet was disrupted in the transition-state model, and as a result the distance between Lys 27 and His 102 increased by >8.5 Å (Figure 9). The disruptions of core 2 also led to the loss of interactions of loop 4. Loop 5, in contrast, was maintained in all transition states with Cα RMS deviations of 0.2−0.4 Å to the NMR structure.

Since the transition state is made up of an ensemble of structures, another independent wild-type simulation was performed to better sample this ensemble as well as to check the reproducibility of our findings. The transition state identified in the second simulation is similar to the wild-type transition discussed above. For example, the secondary structure contents and solvent accessibilities are similar (compare the WT TS1 and WT TS2 entries in Table 1). The second transition state is also approximately 5 Å from the native state. However, there are also some differences between the two transition states, and the RMS deviation between the two average transition state structures is 5.4 Å. The heterogeneity of the simulated transition states is illustrated by snapshots taken at 1-ps intervals from the transition-state ensembles in Figure 10 (TS1 is in red and TS2 is in green). While the transition states share many features, they are distinct.

Owing to the difficulty in defining and identifying transition states in MD simulations, a more quantitative comparison to experiment is necessary. The transition state of the wild-type protein has been studied experimentally, and its structure is inferred from the quantity Φ. To compare with experiment, we use a structure index that describes the secondary and tertiary structure at each residue along the sequence in the transition-state model [$S = S_{2^\circ}S_{3^\circ}$, where S_{3° is the extent of tertiary contacts and S_{2° is the percentage of local secondary structure; for further discussion, see Daggett et al.[17] and Li and Daggett[29]]. The S values calculated from the wild-type transition-state model and the Φ_F values determined experimentally[4,6,30] are given in Figure 11. The agreement between the two approaches is good, with the exception of α2 (Figure 11A). The correlation coefficient between the two sets of independently obtained data is 0.75 for wild-type TS1; however, the correlation improves to 0.84 if the outlier depicted by the square (residue 32) is removed (Figure 11B). The effects are more dramatic if all α2 residues are excluded, $R = 0.93$ (Figure 11C).

Discussion

Simulations of the thermal denaturation of barnase in water was performed with the aim of identifying and characterizing the transition state of unfolding. The transition states were identified on the basis of the rate of structural change and other conformational analyses, as described previously for chymotrypsin inhibitor 2.[15,16] The wild-type transition state occurred early in the two independent simulations (135−140 ps for TS1

(30) Matouschek, A.; Serrano, L.; Fersht, A. R. *J. Mol. Biol.* **1992**, *224*, 819−835.

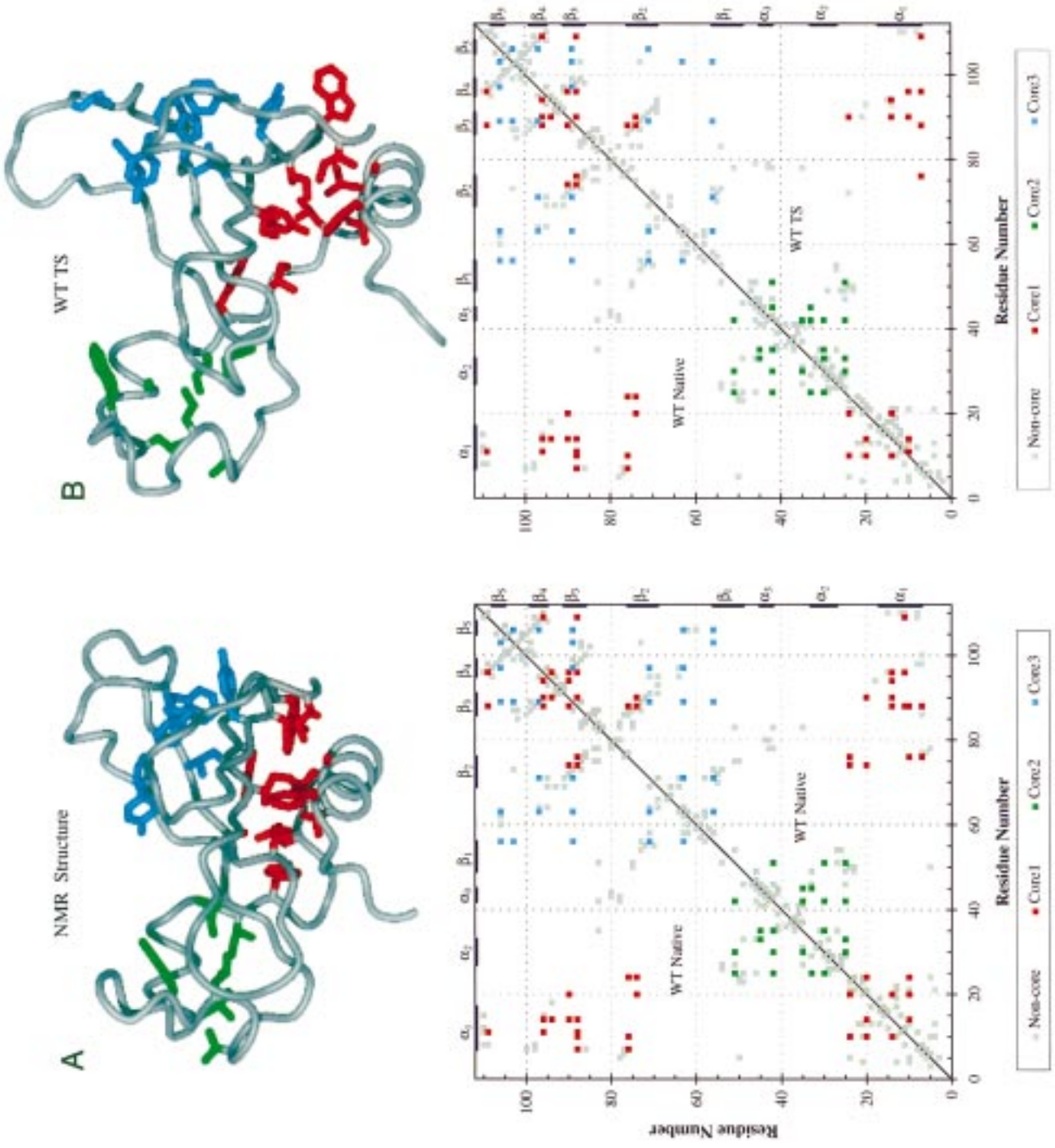
A
NMR Structure
B
WT TS
WT Native
WT TS
Residue Number
Non-core
Core1
Core2
Core3

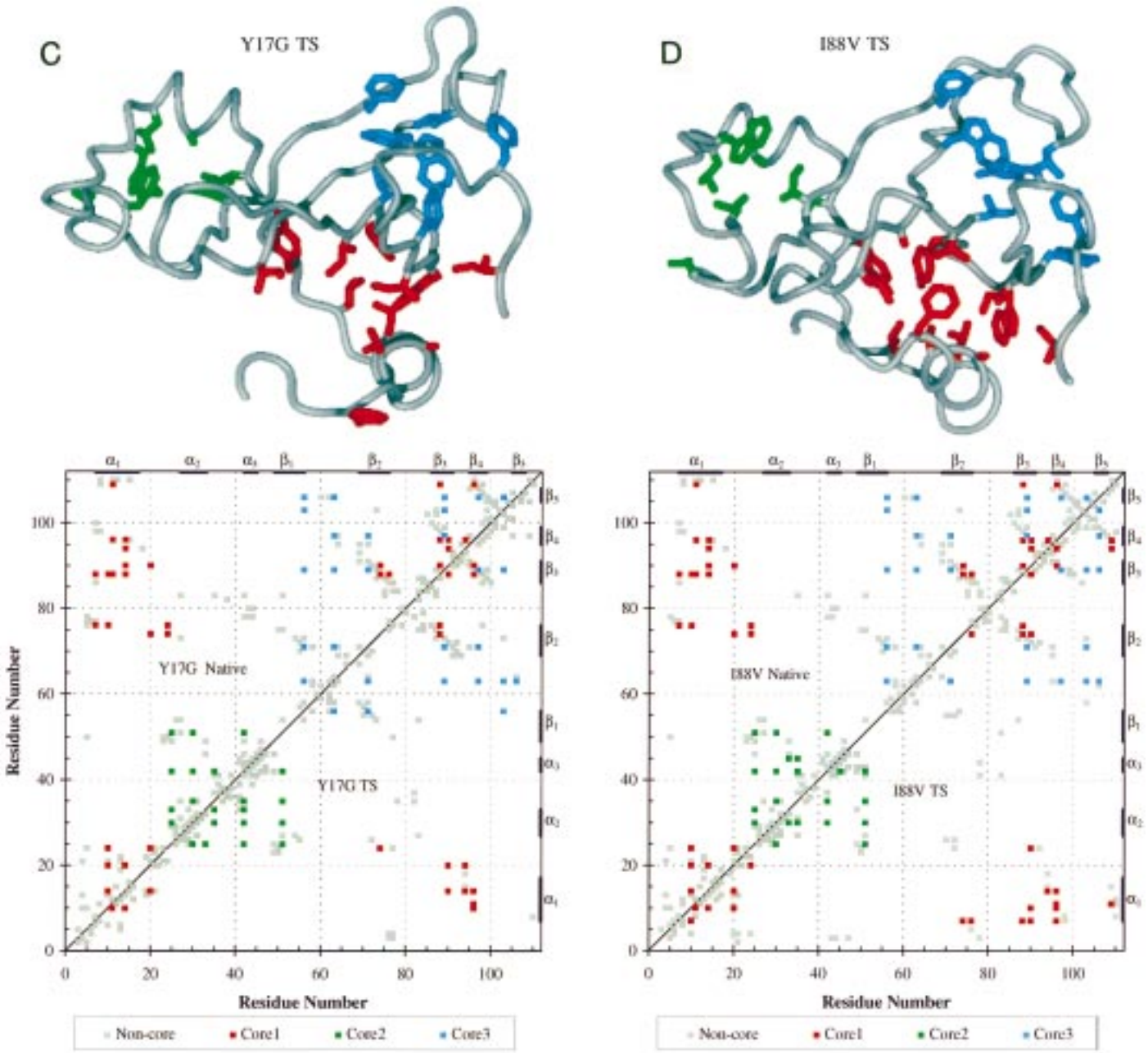

Figure 8. Packing in the hydrophobic cores in the average NMR structure and the average transition-state structural models. For clarity, only core residues are displayed: red, core 1; green, core 2; and blue, core 3. The same coloring scheme is used in the side-chain contact maps. The tertiary contacts were calculated on the basis of heavy atom contacts between nonneighboring residues.[16]

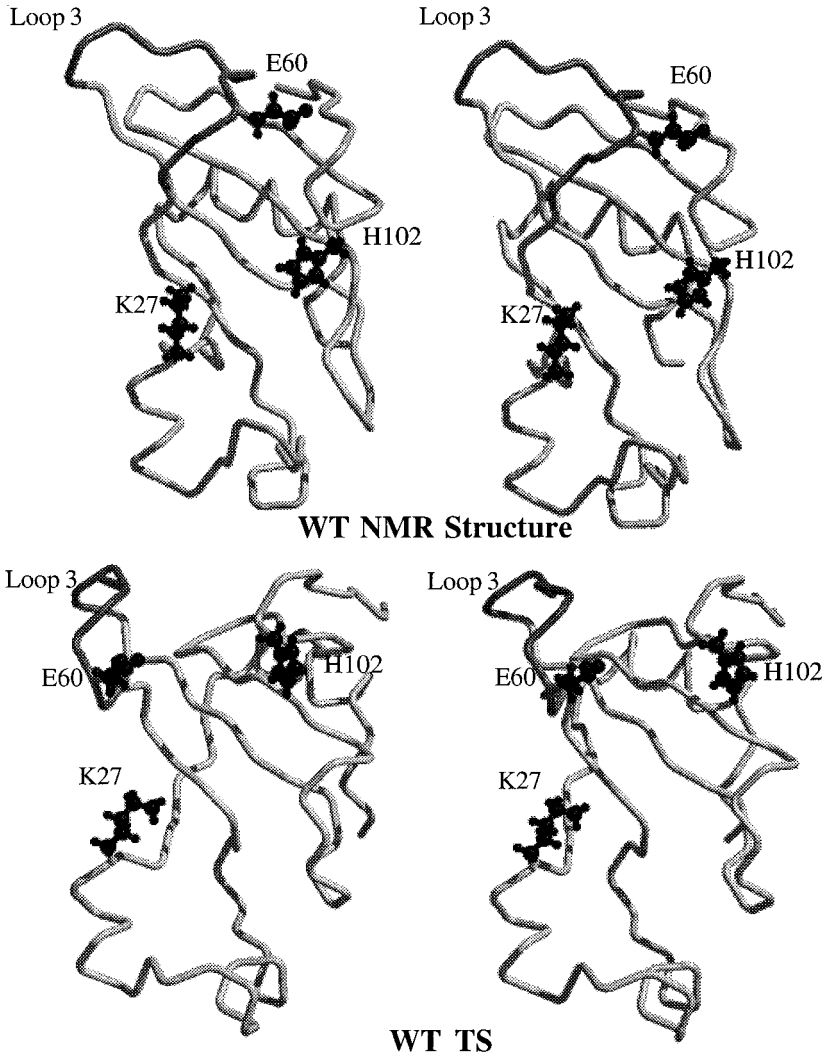

Figure 9. Stereoview of the native and transition-state structures for the wild-type protein, highlighting the loop motion.

and 185−190 ps for TS2). The transition state can be described as a distorted form of the native state with disrupted packing interactions, distorted loops, and frayed secondary structure. Later time points in the wild-type simulation provide structural models for the major intermediate state[29] and the denatured state[31,32] that are in agreement with experiment. We now complete the description of the unfolding of barnase by characterization of the transition state. Simulations of two mutants were also performed to address the effect of mutation on the unfolding pathway and major transition state. The I88V and Y17G mutations were chosen because I88V is a relatively conservative mutation that has little effect on the structure of the transition state, based on experiment.[33] In contrast, Tyr 17 → Gly causes more drastic changes to the transition state and displays both Hammond and anti-Hammond behavior.[6] The Hammond effect is attributed to movement of the transition state along the reaction coordinate toward the native state. The anti-Hammond effect is described as movement of the transition state along the energy surface perpendicular to the reaction coordinate. Such effects are difficult to visualize for something as complicated as a transition state for folding, and it is our goal to obtain detailed molecular models to provide a structural framework for the experimentally observed sensitivity and movement of the transition state upon mutation.

Effect of Mutations on the Unfolding Pathway. In all three proteins simulated, there was early expansion of the molecule with some loss of secondary structure, particularly fraying of the helices and the edges of the β-sheet. This progression has also been seen in other denaturation simulations of barnase by Caflisch and Karplus.[34,35] Some α-helical structure was present throughout the wild-type and I88V simulations. In the case of α1, the helix completely unfolded but refolded over time.[31,32] The unfolding proceeded from the N-terminus, as has also been observed by Caflisch and Karplus[35] and in simulations of α1 peptide fragments.[32] The main difference between wild type and I88V was that the mutation caused local disruptions to the packing of core 1, leading to faster unfolding of the secondary structure but via the same path as for the wild-type protein.

The initial steps in the unfolding of Y17G were similar to those of wild type and I88V, except that there was a much greater loss of the helical structure from α1. A Tyr → Gly mutation in a helix is expected to lead to loss of helical structure,

(31) Bond, C. J.; Wong, K. B.; Clarke, J.; Fersht, A. R.; Daggett, V. *Proc. Natl. Acad. Sci. U.S.A.* **1997**, *94*, 13409−13413.
(32) Wong, K. B.; Clarke, J.; Bond, C. J.; Neira, J. L.; Freund, S. M. V.; Fersht, A. R.; Daggett, V. *J. Mol. Biol.*, submitted.
(33) Dalby, P. A.; Oliveberg, M.; Fersht, A. R. *J. Mol. Biol.* **1998**, *276*, 625−646.
(34) Caflisch, A.; Karplus, M. *Proc. Natl. Acad. Sci. U.S.A.* **1994**, *91*, 1746−1750.
(35) Caflisch, A.; Karplus, M. *J. Mol. Biol.* **1995**, *252*, 672−708.

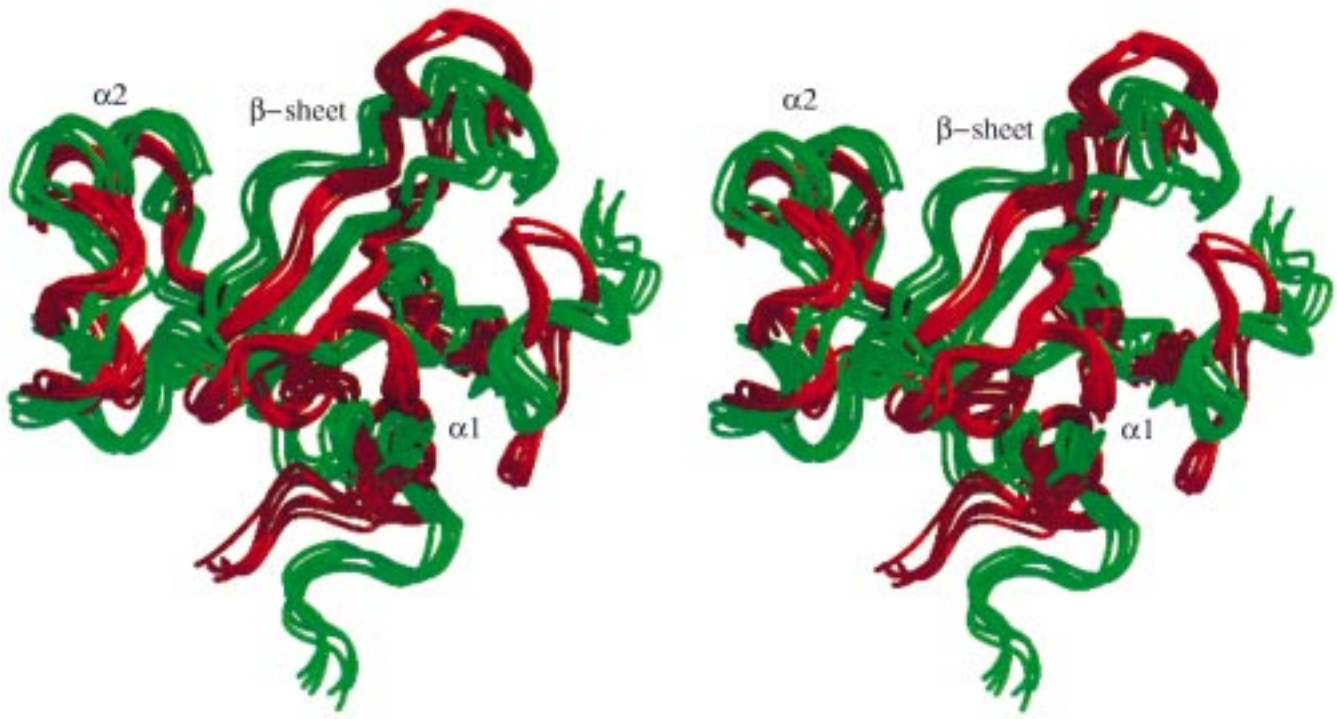

Figure 10. Stereoview of 1-ps snapshots of the wild-type transition-state ensembles, TS1 (beginning from the NMR structure, the major wild-type simulation, in red) and TS2 (beginning from the crystal structure, in green), to demonstrate the heterogeneity of the transition state. Six structures are given for each ensemble.

given the added flexibility of Gly, the disruption of packing interactions, and the differences in the helical propensities of Tyr and Gly, particularly at the C-terminus of a helix. However, disruption of the helix was not localized to the site of the mutation. Instead, it unfolded from the N-terminus, as it does in the wild-type protein (Figure 6), although some minor distortions about residue 17 were evident. The C-terminal portion of α1 appears to be inherently more stable than the N-terminus and is partly retained in the denatured state of the wild-type protein, as has been observed by NMR[36,37] and simulation.[31,32] In any case, the Y17G mutant initially followed a path similar to wild type but quickly diverged and lost nearly all α-helical structure (Figure 3). This mutant contained the lowest helix content at the end of the simulations (Figures 2B, 3, and 4).

Wild-Type Transition-State Ensemble. The simulated transition-state ensemble had the following characteristics: tertiary packing interactions were weakened relative to those in the native state; α1 and α2 were essentially intact; the core of the *β*-sheet was intact; and the loops were disrupted (Table 1, Figures 7, 8, and 10). The average structure of the transition state has a RMS deviation of ∼5 Å from the native state, which is comparable to the differences between the wild-type transition-state ensembles (Table 1, Figure 10). Overall, the transition-state ensemble of barnase can be viewed as a collection of related structures representing an expanded and distorted form of the native state. Such a state is expected to represent a high free energy barrier because of the loss of favorable packing interactions and some secondary structure without considerable compensation from heightened mobility, or an increase in entropy, as seen in later more unfolded structures.

While the simulated transition-state ensembles are comprised of different structures (that differ by approximately 5 Å), they are related. For example, 40% of the residues with high *S* values ($S > 0.75$) in TS1 are also high in TS2. In TS2, 71% of the residues with high *S* values are also high in TS1. This correspondence is to be expected because some of the regions of the protein are highly structured by both MD and experiment, and this structure will constrain the degree of heterogeneity attainable by the transition-state ensemble. But, our sampling is necessarily limited, and the inclusion of more simulations has been shown to broaden the transition-state ensemble,[16,38] but wildly divergent structures were not observed. Lazaridis and Karplus[39] have reported similar average results in multiple all-atom simulations of CI2. In contrast, low-resolution lattice simulations on a $3 \times 3 \times 3$, or 27-mer, cubic lattice with three designated bead-types (or residue types), for which exhaustive sampling of conformations is possible, have led to the conclusion that the transition-state ensemble is highly heterogeneous.[40] Guo and Thirumalai[41] have reached similar conclusions using a 46-mer, off-lattice model. In their system, the folding nucleus was neither specific nor unique. In contrast, Abkevich et al.[42] have suggested that the critical nucleus, the assumed transition-state, is specific and sufficient for folding with some sequences on lattices. The high degree of heterogeneity observed with many simple models may be due to the reduced sequence, with respect to both polymer length and character, as acknowledged by Onuchic and co-workers,[40] who say that conclusive results will be provided by simulations of real proteins. That is, the transition states from simple models may become more specific when the

(36) Arcus, V. L.; Vuilleumier, S.; Freund, S. M.; Bycroft, M.; Fersht, A. R. *J. Mol. Biol.* **1995**, *254*, 305−321.
(37) Freund, S. M. V.; Wong, K.; Fersht, A. R. *Proc. Natl. Acad. Sci. U.S.A.* **1996**, *93*, 10600−10603.
(38) Kazmirski, S. L.; Daggett, V. *J. Mol. Biol.* **1998**, *277*, 487−506.
(39) Lazaridis, T.; Karplus, M. *Science* **1997**, *278*, 1928−1930.
(40) Onuchic, J. N.; Socci, N. D.; Luthey-Schulten, Z.; Wolynes, P. G. *Folding Des.* **1996**, *1*, 441−450.
(41) Guo, Z.; Thirumalai, D. *Folding Des.* **1997**, *2*, 377−391.
(42) Abkevich, V. I.; Gutin, A. M.; Shakhnovich, E. I. *Biochemistry* **1994**, *2*, 10026−10036.

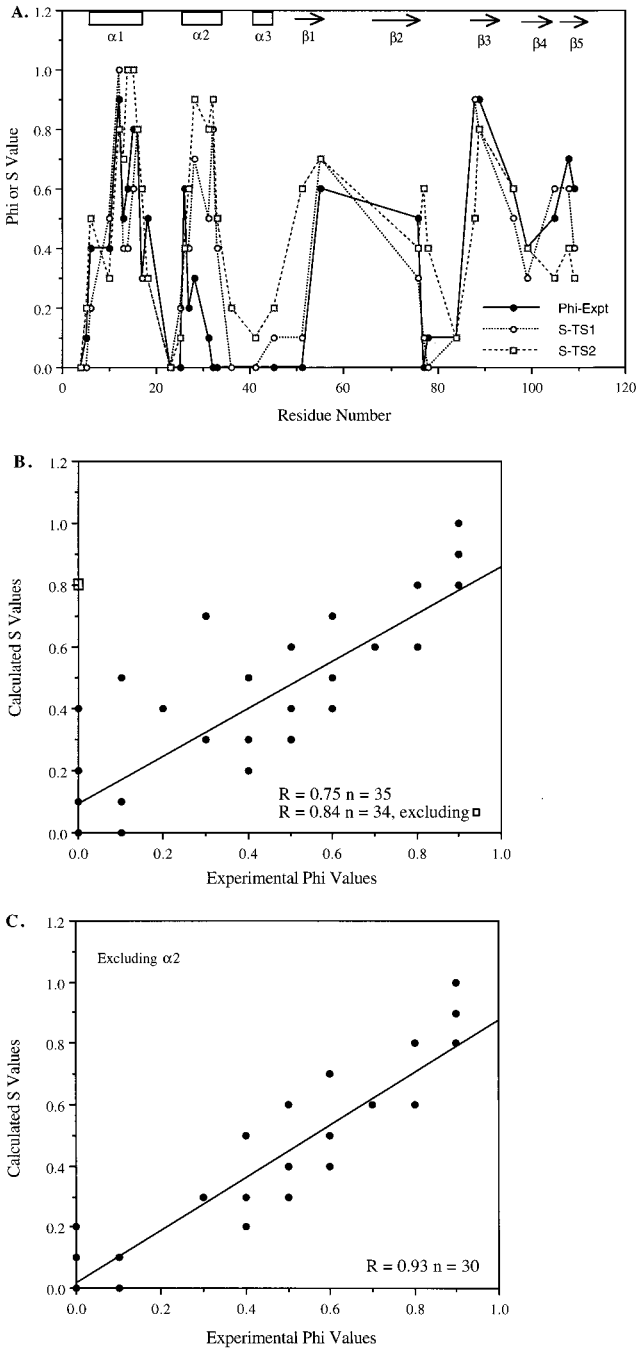

Figure 11. (A) Variation of the experimental Φ-values and the calculated *S* values for the two wild-type transition-state models along the sequence. The simulated native state was used as the reference state for calculation of the *S* values. Further details regarding calculation of *S* values and the properties of the simulated native state have been described by Li and Daggett.[29] (B and C) Comparison of the experimental Φ-values and calculated *S* values for the main transition-state model (TS1) described in the text.

actual protein sequences, including side chains, are used and exert further constraints to limit the allowable conformations.

As mentioned above, the transition-state ensembles from the MD simulations were identified by analyzing conformational properties of the protein as it unfolded, not free energies. Also, we note that the MD-generated ensembles were generated at very high temperature (225 °C). As in a real experiment, one must destabilize the native state to monitor unfolding, and such a high temperature is necessary to accelerate the unfolding process so that it occurs on the nanosecond time scale. High temperature should only change the population of different pathways, and those that are accessible at low temperature are still accessible at high temperature. While we do not have experimental data up to 225 °C, Dalby et al.[43] have found that the "average" structure of the transition state does not appear to change as the temperature is varied up to 50 °C. Despite the high temperature in the simulations, conformational sampling is limited compared to the much vaster ensembles probed by experiment. As such, we hope that MD can capture the dominant properties of the transition state, but we do not expect to reproduce all aspects of the true transition state. In any case, due to these limitations, the resulting MD-generated structures are viewed as testable models that *must* be validated by comparison with experiment.

Sancho et al.[44] have developed a method for probing interactions between active-site residues and ligands in the transition state by monitoring the effect of 3′-GMP on the rate constants of unfolding wild-type and mutant forms of barnase. Using this approach, they determined that interactions between His 102 and the ligand are maintained in the transition state, and interactions with Glu 60 are partially maintained, while those with Lys 27 are essentially lost. Therefore, the active site is partly retained in the transition state. In our wild-type transition-state models, the position of His 102 relative to the floor of the active site formed by the β-sheet was retained (Figure 9). Loop 3 moved down toward the center of the protein, shifting Glu 60, but Glu 60 and His 102 remain near in space, spanning the active-site cleft. The docking between the N-terminal end of α2 and the β-sheet was disrupted in the transition-state model, and as a result, the distance between Lys 27 and His 102 increased by >11 Å.

Despite the expansion and increase in solvent-exposed surface area, there was little to no water in the core of the transition state, and the nonpolar core residues remained sequestered from solvent (Figure 8). Oliveberg and Fersht[45] have measured the change in heat capacity, ΔC_p, for the TS → D and N → D transitions. The resulting values are similar, suggesting that there is little change in water interactions with the nonpolar groups in the N → TS transition and that the transition-state is relatively "dry".

A more detailed comparison with experiment is provided by a residue-based structural analysis of the simulated transition-state ensemble for comparison with Φ_F values obtained using the protein engineering method.[4,6,29] To this end, a structure index was computed for each residue on the basis of the local secondary and tertiary structures of the transition-state models relative to the native state, as described by Daggett et al.[17] and Li and Daggett.[29] The degree of structure along the sequence is reproduced by both of the independent wild-type transition-state models, with the exception of α2 (Figure 11A). The models appear to overestimate the structure in α2, which according to experiment should be extremely weak to nonexistent (Figure 11A). The correlation between the experimental and calculated values is good (R = 0.75 or 0.84 for TS1, Figure 11B). Excluding α2 from the comparison results in a correlation coefficient of 0.93. Thus, almost all major trends are reproduced by the models of the wild-type transition state, with high degrees of structure in α1 and the central strands of the β-sheet and moderate, but still significant, amounts of structure in the edge strands (Figures 7 and 11).

(43) Dalby, P. A.; Oliveberg, M.; Fersht, A. R. *Biochemistry* **1998**, *37*, 4674−4679.
(44) Sancho, J.; Meiering, E. M.; Fersht, A. R. *J. Mol. Biol.* **1991**, *221*, 1007−1014.
(45) Oliveberg, M.; Fersht, A. R. *Biochemistry* **1996**, *35*, 2738−2749.

Discrepancy between Simulation and Experiment for α2: A New Twist to Φ-Values. The Φ-values for α2 are among the most reliable determined, being derived from very careful "Ala → Gly scanning" experiments.[6] The simplest answer to the discrepancy is that the simulations overestimate the strength of the interactions in α2. However, NMR studies show that the backbone NH groups of Ala 32 and Leu 33 are protected early in folding, before the folding transition state.[46] In addition, both experiment and simulation indicate that α2 adopts a significant amount of helical structure in the denatured state.[31,32,36,37]

Further aspects of the simulation suggest a reconciliation of all the data. The region of structure containing α2 is pinched off from the rest of the protein in the simulated transition, intermediate,[29] and denatured states,[31,32] such that the folding of α2 could be semi-autonomous. If α2 folds independently, then the effect of mutations may be not be felt by the rest of the protein until significant interactions are made with α2, which does not occur until after the transition state for folding. This twist of analysis could potentially occur for any multimodular protein where portions of the structure could fold semi-autonomously. Such an effect is unlikely for a single "foldon" such as CI2, and we note that the Φ values from theory and experiment are in very good agreement for the transition state of CI2.[8,9,15−18]

Effect of Mutations on the Transition State of Unfolding. Aside from possible complications involving α2, the wild-type transition-state structures appear to be good models for the transition state of unfolding of barnase. It is then of interest to investigate the effects of mutations on the transition-state. One assumption of the protein engineering method, as employed for Φ-value analyses, is that mutations do not affect the folding/unfolding pathway and instead are merely probes of the structure, which is also an assumption inherent in the comparison of the *S* and Φ values. Simulations of mutant forms of barnase, such as I88V, provide a test of this assumption. Gross movement of the transition state upon mutation in the form of both Hammond and anti-Hammond effects has been detected by β_T values.[5,6] The effect of mutations on the unfolding pathway was addressed above, and the simulations can also be used to describe the changes that give rise to the observed movement of the transition state.

The effect of mutations on the transition-state can be evaluated by comparing the interactions involving the mutant residue in *its* simulated transition-state structures and the wild-type residue in *its* transition-state ensemble. While the transition-state models may not uniquely or comprehensively represent all aspects of the true transition-state ensemble, they are in good agreement with experiment and appear, therefore, to be plausible structural models of this state. The I88V control mutation supports the central assumptions of the protein engineering method that mutations are merely probes of the transition state and do not make or break interactions appreciably. The I88V mutation led to faster unfolding of the protein and local disruptions of the transition state structure, but the wild-type and I88V transition state structures were similar overall (Table 1, Figure 7) and within the envelope of transition state structures that result from pooling the ensembles from multiple wild-type simulations, as was done for chymotrypsin inhibitor 2[16] and here in a more limited way (Table 1, Figure 10). Interestingly, the local packing defects caused by the mutation were compensated elsewhere. Specifically, tertiary interactions in core 2 were disrupted in the I88V transition state relative to wild type, but

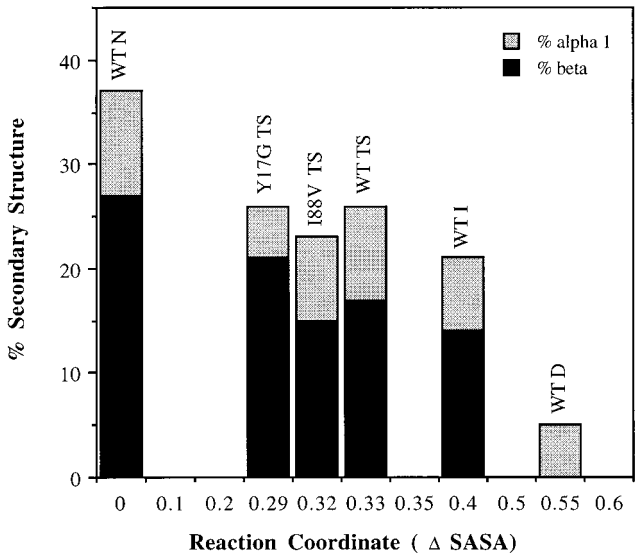

Figure 12. Percentage of secondary structure in different conformational states of the wild-type and mutant proteins as a function of a reaction coordinate based on the change in solvent-accessible surface area of the models relative to the native state. Values are taken from Table 1, except that the secondary structure content is the percentage of the sequence that is ordered (i.e., the secondary structure content in Table 1 divided by 107, which is the number of dihedral pairs in barnase because the first residue is undefined in the crystal structure). Note that the *x*-axis is not uniform.

there was an increase in contacts in core 1 (Figure 8). Overall, this mutation introduced mostly local defects to core 2, but some minor longer-range effects were also evident.

While the Y17G transition state is similar to the wild-type transition-state in terms of many of its overall properties (Table 1, Figure 7), the secondary structure is different. In particular, the β-structure is more ordered and α1 is more disrupted in the transition state (Figure 9, Table 1, and discussed above). The mutation at the C-terminus led to loss of helix at the N-terminus, as discussed above (65-ps structure in Figures 6 and 7). Matthews and Fersht[6] have investigated the effect of the Y17G mutation on the structure of α1 by constructing a double mutant, such that the Y17G mutant is the reference state. Using this approach, they found that the Φ value for an Ala → Gly mutation at residue 12 drops from 0.9 in wild type to 0.2 in the double mutant, indicating that there was a substantial loss of structure upstream from position 17, as observed in the simulations (Figures 6 and 7). As with I88V, Y17G displayed compensation in packing interactions, such that there were slight improvements in the packing of cores 2 and 3, although local interactions in core 1 were disrupted upon mutation (Figure 8).

In addition, the solvent-accessible surface area of the Y17G transition-state was lower than those of wild type and I88V (Table 1). These results are consistent with the percentage change in solvent-accessible surface area as reflected by the $m_{‡-D}/m_{N-D}$ values determined experimentally (Table 1). As mentioned above, this ratio is analogous to a Brønsted β, or Tanford β_T, value and thus serves as a measure of the position of the transition state along the reaction coordinate. Various states from the simulation are ordered by their accessible surface area relative to the NMR structure in Figure 12. By this measure, the transition state of Y17G is closer to the native state than the wild-type transition state (Figure 12). However, for the Y17G transition state, the helical content of α1 is lower and the β-content is significantly higher (Table 1). I88V is very similar to wild type although a slight loss of both α- and β-structure is

(46) Matouschek, A.; Serrano, L.; Meiering, E. M.; Bycroft, M.; & Fersht, A. R. *J. Mol. Biol.* **1992**, *224*, 837−845.

evident (Figure 12, Table 1). Therefore, the Y17G transition-state is more nativelike with respect to its overall structure and in terms of β-structure, as is expected for a Hammond effect. At the same time, the helical structure is disrupted, as for the anti-Hammond effect. Thus, the simulations provide a tangible structural framework for interpretation of the transition-state effects observed experimentally.

Acknowledgment. We are grateful for financial support from the National Institutes of Health (GM 50789 to V.D.). Figures 1, 4, 6, and 7 were made using Raster3D[47,48] and/or Molscript,[49] and Figures 8 and 9 were made using UCSF MidasPlus.[50]

JA981558Y

(47) Bacon, D. J.; Anderson, W. F. *J. Mol. Graphics* **1988**, *6*, 219−220.
(48) Merritt, E. A.; Murphy, M. E. P. *Acta Crystallogr. Sect. D* **1994**, *D50*, 869−873.
(49) Kraulis, P. J. *J. Appl. Crystallogr.* **1991**, *24*, 946−950.
(50) Ferrin, T. E.; Huang, C. C.; Jarvis, L. E.; Langridge, R. *J. Mol. Graphics* **1988**, *6*, 13−27.
(51) Kabsch, W. *Acta Crystallogr. Sect. A.* **1976**, *32*, 922−933.
(52) Daggett, V.; Kollman, P. A.; Kuntz, I. D. *Biopolymers* **1991**, *31*, 1115−1134.
(53) Daggett, V.; Levitt, M. *J. Mol. Biol.* **1992**, *223*, 1121−1138.
(54) Hubbard, S. J.; Thornton, J. M. *NACCESS, Computer Program*; Department of Biochemistry and Molecular Biology, University College, London, 1993.